ELSEVIER

CrossMark

BRACHYTHERAPY

Brachytherapy 22 (2023) 80–92

A versatile physical phantom design and construction for I-125 dose measurements and dose-to-medium determination

Paula Cristina Guimarães Antunes*, Paulo de Tarso Dalledone Siqueira, Julian Barbosa Marco Shorto, Hélio Yoriyaz

Instituto de Pesquisas Energéticas e Nucleares – IPEN-CNEN/SP, São Paulo, Brazil

ABSTRACT

PURPOSE: In this paper we present a phantom designed to provide conditions to generate set of "true" independent reference data as requested by TG-186, and mitigating the scarcity of experimental studies on brachytherapy validation. It was used to perform accurate experimental measurements of dose of ^{125}I brachytherapy seeds using LiF dosimeters, with the objective of experimentally validating Monte Carlo (MC) calculations with model-based dose calculation algorithm (MBDCA). In addition, this work intends to evaluate a methodology to convert the experimental values from LiF into dose in the medium.

METHODS AND MATERIALS: The proposed PMMA physical phantom features cavities to insert a LiF dosimeter and a ^{125}I seed, adjusted in different configurations with variable thickness. Monte Carlo calculations performed with MCNP6.2 code were used to score the absorbed dose in the LiF and the dose conversion parameters. A sensitivity analysis was done to verify the source of possible uncertainties and quantify their impact on the results.

RESULTS: The proposed phantom and experimental procedure developed in this work provided precise dose data within 5.68% uncertainty ($k=1$). The achieved precision made it possible to convert the LiF responses into absorbed dose to medium and to validate the dose conversion factor methodology.

CONCLUSIONS: The proposed phantom is simple both in design and as in its composition, thus achieving the demanded precision in dose evaluations due to its easy reproducibility of experimental setup. The results derived from the phantom measurements support the dose conversion methodology. The phantom and the experimental procedure developed here can be applied for other materials and radiation sources.

Keywords: Brachytherapy; Phantom; Dosimetry; ^{125}I seed, LiF; Dose-to-medium; Monte Carlo

Introduction

Thermoluminescent dosimeters (TLDs) have been applied to quality assurance (QA) and *in vivo* measurements connected to several radiotherapy techniques for a century now (1). These dosimeters are tissue equivalent and sensitive to a wide dose range of different radiation types, depending on their chemical composition. In addition, they are both long-term and widely commercially available, being still the most applied to measurements in radiation therapy (2).

Since TLDs are secondary dosimeters, their sensitivity to dose is determined by measuring their response to a known dose delivered by a calibrated reference beam. Such calibration is frequently made in a ^{60}Co or MV photon beam to assure traceability to primary standards for absorbed dose to water (3). To measure the absorbed dose from low-energy photons in experimental procedures, as in brachytherapy (BT), one needs to perform a correction procedure to cope with the TLD response difference between beam quality at calibration and at measurement (3–6). Several studies describe the complexity of using TL dosimetry for low-energy sources and quantify such energy dependencies, recommending universal corrections based on primary standards and dosimetry protocols (7–13).

Received 29 June 2022; received in revised form 15 September 2022; accepted 9 October 2022

Disclosure: The authors report no proprietary or commercial interest in any product mentioned or concept discussed in this article.

* Corresponding author. Instituto de Pesquisas Energeticas e Nucleares – IPEN-CNEN/SP, Nuclear Engineering Center, Av. Prof. Lineu Prestes, 2242, 05508000, Sao Paulo, Brazil. Tel: +55 11 2810-5732.

E-mail address: pacrisguian@gmail.com (P.C.G. Antunes).

1538-4721/$ - see front matter
https://doi.org/10.1016/j.brachy.2022.10.005

Despite the required experimental complexity to perform TLD dosimetry, the high sensitivity and small dimensions make TLDs of LiF:Mg,Ti an excellent choice for experimental evaluations in high dose gradient regions, such as in BT at short distances from the seed (14−16). Not surprisingly, several studies based on *in vivo* dosimetry highlight LiF TLDs as one of the main dosimeters in BT, since they allow the quantification of dose in regions where the treatment planning systems (TPS) is inaccurate. In regions such as the skin, for example, the TPS overestimates the absorbed dose because it does not consider the finite patient dimensions and assumes a homogeneous water medium (17−19).

In this sense, QA routine in BT procedures still follow dosimetry formalism recommended by the American Association of Physicists in Medicine (AAPM) – Task Group report No. 43 (TG-43) (3), introduced in 1995 and subsequently modified in various publications: 2004 update TG-43U1 (4), 2007 supplement TG-43U1S1 (5) and 2017 supplement 2 TG-43U1S2 (6), the latter used as reference in this study. This formalism assumes water as the standard dosimetry medium, so all calculations are performed around a seed embedded in an infinite water medium.

In contrast, in BT clinical practice the model-based dose calculation algorithm (MBDCA) was introduced to perform dose calculations in conditions closer to reality and to improve dose delivery accuracy (20,21). These algorithms propose dose estimates directly into medium and have been introduced in some commercial TPS such as ACE[1] (22,23) and ACUROS™ [2] (24,25) for high-dose-rate (HDR) applications with ^{192}Ir.

With the advent of dose calculation in the medium, the TG-186 (21) describes three different ways of reporting the absorbed dose: $D_{w,w}$ - absorbed dose to water in water; $D_{w,m}$- absorbed dose to water in medium and; $D_{m,m}$ - absorbed dose to medium in medium. In addition to these notations, when it comes to experimental dosimetry new notations are needed (26), since the dose will be deposited in the dosimeter. This way, for experimental measurements with LiF dosimeters: $D_{LiF,w}$ and $D_{LiF,m}$ (absorbed dose to LiF in water and medium, respectively). The correlation between dose estimates in different media is obtained through the cavity theory. Different approaches of such correlation have been the subject of some recent publications, see Beaulieu *et al.* (21), Branco *et al.* (26), Andreo (27,28), Ballester *et al.* (29), Giménez-Alventosa *et al.* (30) and references therein.

Despite the importance of experimental dosimetry in detecting errors, in clinical procedures or in dose calculations, experimental BT validation studies are still scarce and limited. In recent years, the main experimental data were based on TG-43, with the characterization of BT sources in an infinite medium of water, generating data used as a reference in clinical routine (6,14,16,31,32).

However, with the change of perspective in the way of estimating the dose, $D_{m,m}$, new complexities were added to the experimental procedures, especially for low-energy BT, such as ^{125}I, ^{103}Pd and ^{131}Cs seeds. Since the composition of the medium is more significant in this energy range, due to the predominance of the interaction of radiation by photoelectric effect (21,24).

The main current studies seek to determine $D_{m,m}$ by calculation, however, there is a lack of information and details regarding experimental values with LiF and their conversion to $D_{m,m}$. This is due to the difficulty of obtaining accurate measurements and the lack of reference for a precise and practical dose conversion method. Keeping that in mind, this work addresses two main objectives: (a) propose a physical phantom that respects the premises presented by TG-186, based on a simple configuration that allows dosimetry evaluations with reduced uncertainties and control of the studied processes. This phantom was used to perform ^{125}I seed dose profile measurements with LiF dosimeters in order to validate experimentally the Monte Carlo (MC) calculations with MBDCA; (b) convert the experimental LiF dose into absorbed dose to medium in medium ($D_{m,m}$) using the cavity theory and MC calculations.

Methods and materials

Proposed phantom

Figure 1 shows the physical phantom geometry developed in this work. It consists of a set of three square (100×100 mm^2) polymethyl methacrylate (PMMA) sections, which are assembled one over another. The first section consists a 10.0 mm thick slab with a LiF holder cavity on the center of its top surface; the second section consists of one or more PMMA slabs forming a section with variable thickness (z); the third section is a 10.0 mm thick superior slab with a ^{125}I holder cavity on the center of its bottom surface.

Ten phantoms were used simultaneously in the experimental procedure carried on along this work. Fourteen PMMA squared slabs of different thicknesses were used interchangeably, alone or arranged in groups, to set the source-detector distances (second section). Table 1 shows the different slabs used (a-n) and their thickness, as well as the arrangements to form the second section of thickness (z).

The PMMA specification given by the manufacturer are: atomic composition (H, C, O) = (8.0538 %, 59.9848 %, 31.9614 %), $Z_{eff} = 6.53$ and mass density $\rho = 1.19$ g/cm^3. The mass density value was confirmed by experimental measurement, resulting in 1.18 ± 0.02 g/cm^3, with excellent agreement with the manufacturer-stated value.

[1] (Advanced calculation engine – Nucletron – an Elekta Company, Veenendaal, The Netherlands)

[2] (Transpire Inc., Gig Harbor, WA)

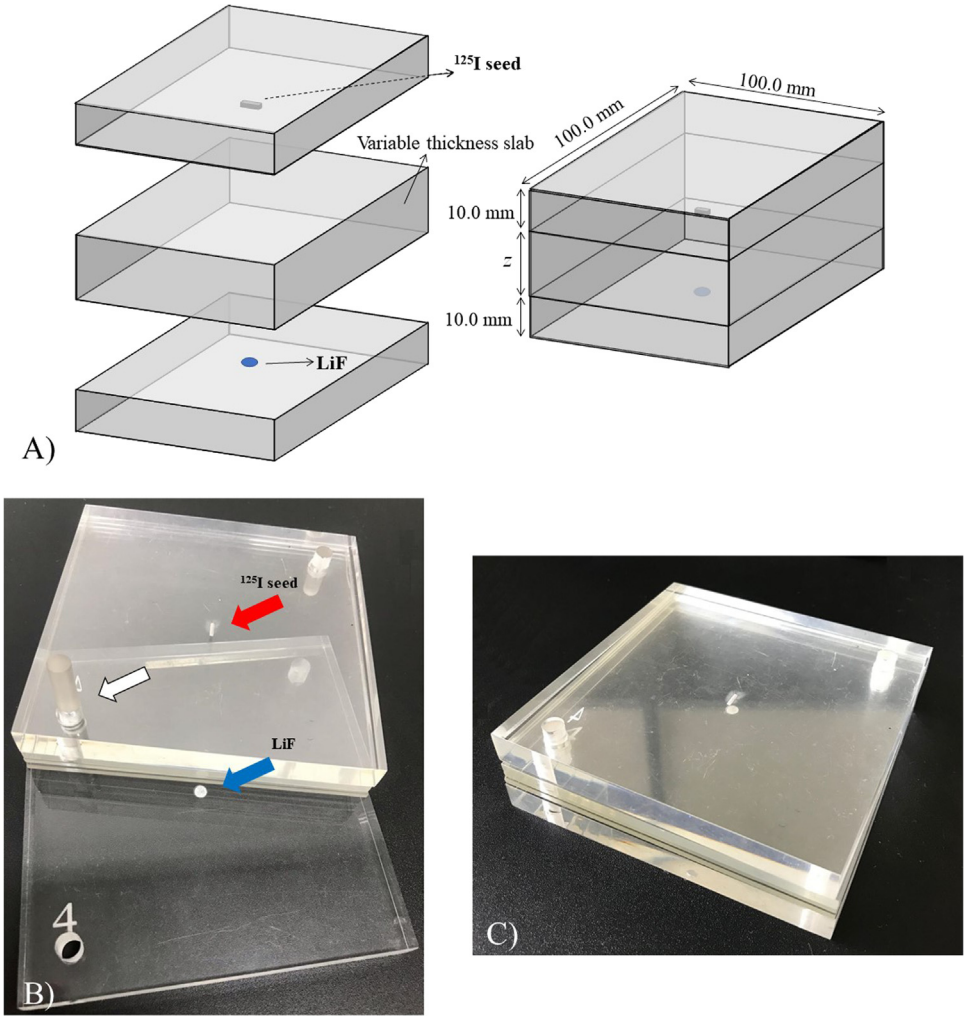

Fig. 1. (a) Schematic illustration of the phantom. (b) Picture of the phantom, with red and blue arrows showing PMMA slabs with ^{125}I seed and LiF, respectively. The white arrow shows the lateral pin used to align the slabs. (c) Phantom arranged in its irradiation configuration. (For interpretation of the references to color in this figure legend, the reader is referred to the Web version of this article.)

PMMA is the only material used in the phantom due to its low cost and easy handling, however, the present phantom can be easily adapted to support heterogeneous materials which shall be presented in a subsequent work. Two PMMA pins, located at two opposite corners of the phantom were used to hold and align the slabs, ensuring immobilization during irradiation, and the proper relative positioning of the seed to the LiF.

Model Amersham 6711 (OncoSeed - GE Healthcare, IL. Marketed by Oncura, Inc) ^{125}I brachytherapy seeds, with initial apparent activities of 1 mCi, were used. Four batches of seeds were used throughout the experiments.

TLD methodology

LiF:Mg,Ti dosimeters (Thermofisher) known as TLD-700 in a disk format of 0.254 mm thick and 3.6 mm in diameter were used in this work. The dosimeters were stored in two separate aluminum trays that were also used for the annealing in a stove. The annealing procedure was similar to that proposed by Davis *et al.* (7). One day before irradiations, the dosimeters were annealed at 400 °C during 1h followed by more 2h at 100 °C on two dedicated stoves. Following the annealing procedure, the dosimeters were cooled to room temperature.

Before the experiments, a batch of 50 LiF was exposed to ^{137}Cs beam inside a 1.0 cm thick rectangular slab PMMA. Three irradiations were performed with 100.0 mGy of air kerma in the position of the dosimeters. Such irradiation allowed the selection of 36 LiF, based on reproducibility (precision < 3.0 %) criteria.

Dose calibration of the LiF response was performed by irradiating 36 selected dosimeters with a dose of 1.0 Gy using a 6 MV X-ray beam produced by a Linac. TLDs were positioned at 5.0 cm depth in an PMMA slab and irradiated with a (10×10 cm^2) field defined at the phantom

Table 1
Variable thicknesses (z) used in the second section with their respective uncertainties, obtained from experimental measurements with a micrometer screw.

Slab		Experimental configuration	
Identification	Thickness (mm)	Arrangement	(z) (mm)
a	1.763 ± 0.016	a	1.763 ± 0.016
b	1.826 ± 0.009	d	2.890 ± 0.014
c	1.872 ± 0.015	e	2.969 ± 0.008
d	2.890 ± 0.014	h	4.020 ± 0.001
e	2.969 ± 0.008	i	4.080 ± 0.014
f	3.858 ± 0.011	j	4.200 ± 0.011
g	3.955 ± 0.001	k	4.300 ± 0.013
h	4.020 ± 0.001	m	5.200 ± 0.011
i	4.080 ± 0.014	$a + b + d$	6.479 ± 0.023
j	4.200 ± 0.011	$c + l$	6.831 ± 0.017
k	4.300 ± 0.013	$a + c + g$	7.590 ± 0.022
l	4.959 ± 0.008	$i + l$	9.039 ± 0.016
m	5.200 ± 0.011	$d + n$	12.640 ± 0.017
n	9.750 ± 0.010	$a + d + f + l$	13.470 ± 0.025

surface, which was positioned at source surface distance (SSD) = 100.0 cm.

LiF reading was performed in a Harshaw 3500 TLD reader one day after the irradiation, so that the trapped charges associated to the low temperature peaks returned to the ground state. The reading parameters used in the analyses were: 10 °C/s heating rate; 60 °C / 400 °C initial/final temperatures and 45 s reading time in a nitrogen gas rich atmosphere. The total area under the TL glow curve was used as the LiF response intensity (I_{LiF}).

The experimental methodology consisted of irradiating the dosimeters in ten phantoms, similar to that shown in Fig. 1, but with different thicknesses of PMMA (z) between the LiF and the ^{125}I seeds, according to Table 1. In all measurements, the irradiation time was adjusted so that the calculated air kerma at 10 cm distance from the seed, in a free vacuum configuration, was 1.5 mGy. Air kerma strength was calculated by the methodology proposed by Taylor *et al.* (33) using small voxel located 10 cm from the seed. Its value was chosen so that the irradiation time span was feasible during the entire seed lifetime. The irradiation time varied from 18 h (at the beginning of seed lifetime) to 47 h (at the end of seed lifetime).

For each irradiation set the background TL signal intensity ($I_{Background}$) was obtained by the average reading of three non-irradiated dosimeters. These dosimeters participated in the annealing and reading procedures along with others. The intensities of these non-irradiated dosimeters were small compared to the irradiated ones. Its relative value depends on the distance between the seed and the irradiated TLDs – less than 0.3% (9.0%) when compared to the intensity from the irradiated dosimeters placed closest (furthest) to the seed.

In this way, the LiF corrected response for a thickness (z), $R_{LiF(z)}$, is given by the equation (1).

$$R_{LiF(z)} = I_{LiF(z)} - \bar{I}_{Background} \quad (1)$$

where $I_{LiF(z)}$ is the response, in μC units, obtained from the TL reader for a LiF placed at a given thickness (z), while $\bar{I}_{Background}$ is the average of the LiF unexposed responses, also given in μC units.

The dosimeters were randomly irradiated several times in the same position, that is, different dosimeters were used to obtain the TLD responses and uncertainties for each thickness (z), resulting in mean values $\bar{R}_{LiF(z)}$. An average of 20 irradiations were performed for each PMMA thickness (z).

Monte Carlo calculations

Monte Carlo (MC) calculations were performed using the Monte Carlo N-Particle – MCNP code version 6.2 (34), which models radiation interactions in matter for the energy range of interest. This code has been successfully applied for dosimetry studies in the brachytherapy field (32,35,36).

The phantom in Fig. 1 was modelled in the code to faithfully reproduce the performed experiments. The ^{125}I seed was modelled according to published descriptions and the primary radionuclide photon emission spectrum was obtained from the USA National Nuclear Data Center (NNDC) (37–39). The mean photon emission energy per ^{125}I decay is 27.4 keV, for the model 6711 seed. This model was validated against dose data available in the literature (data not shown), resulting in a dose rate constant with differences of 0.31 % and 0.95 %, from the data presented in the TG-43 (6) and by Taylor and Rogers (40), respectively. Such differences are within the statistical uncertainties.

Deposited energy and kerma in the LiF were estimated using three different MCNP tallies:

- F4 tally is a track-length estimator and it was used to calculate the fluence of particles in the LiF volume, in 1/cm².source-particle unity. This tally, when associated with the asterisk (*) weights the fluence in energy, resulting in the photon energy-fluence, Ψ. The association of Ψ with the mass energy-absorption coefficients (μ_{en}/ρ), taken from the NIST database, allows the conversion of photon fluence into kerma, in MeV/g.source-particle unity.

- F6 tally is also a track-length estimator and it was used to calculate the kerma, in MeV/g.source-particle unity. This tally performs the same dose calculation as performed by the F4 tally, but using the (μ_{en}/ρ) from MCNP libraries.

- *F8 tally is based on particle collisions and accounts for the energy deposited in the target volume. Rather than using the photon fluence in the target volume to estimate the deposited energy, it tallies the mean energy difference between all incoming and outgoing particles created by each source particle. It was used to estimate the energy deposited in the LiF by particles from the source, in units of MeV/source-particle, obtaining the absorbed dose $D_{LiF,m}$ or $D_{m,m}$ by dividing, respectively by the LiF or medium mass.

Photons and electrons were transported down to a cut-off energy of 1 keV. The number of primary photons was set to 1×10^{10} for all simulations, providing uncertainties below 0.9 % (Type A $\pm$ 1σ). The computational time was approximately 28,000 min, for each simulation run and were performed by a 90 core Intel® Xeon processor. All simulations were performed with MCNP6.2 default parameters, in the standard particle history simulation, that is, a source particle and all its secondary particles generated by it are followed along its history, and no filtering were applied to the tallied results.

MCPLIB 84 and el032 were the cross-section libraries used, in all simulations, to transport photons and electrons, respectively.

Dose to medium from experimental values

Adopting the terminology presented in the TG-43 (6), and assuming that $\bar{R}_{LiF(z)}$ varies linearly with absorbed dose in the studied dose range, the Eq. (2) was used to determine the absorbed dose to medium m, with transport performed in medium m, $D_{m,m}$(16, 32). All data presented in this work use PMMA as the medium (m) in which the radiation is transported. Its specification will be henceforth suppressed to simplify the notation.

$$D_{PMMA(z)}\left(^{125}I\right) = \bar{R}_{LiF(z)}\left(^{125}I\right).N_D(6MV).f^{rel}.k_{bq}^{rel} \tag{2}$$

where $N_D(6MV) = 1/S_D(6MV)$, with $S_D(6MV) = 32.74 \pm 1.25$ μC/Gy, is the absorbed dose calibration coefficient, f^{rel} is the LiF relative absorbed dose energy dependence with respect to the 6 MV calibration beam, k^{rel} is the corresponding relative intrinsic energy dependence of LiFs.

To take into account the different absorbed dose energy dependence of the LiFs in the ^{125}I beam quality and 6MV X-ray, f^{rel} was calculated by MC from Eq. (3).

$$f^{rel} = \frac{f\left(^{125}I\right)}{f(6MV)} = \frac{[D_{PMMA}/D_{LiF}]_{^{125}I}}{[D_{PMMA}/D_{LiF}]_{6MV}} \tag{3}$$

where D_{LiF} is the absorbed dose in the LiF, considering the composition and dimension of the studied dosimeter, and D_{PMMA} is the dose to PMMA at the midpoint of the dosimeter in the absence of the dosimeter, assuming a point detector ($0.1 \times 0.1 \times 0.05$ mm^3). It is necessary to account to $1/r^2$ effect of the beam, which can decrease f^{rel} by up 2.4 % (9). The ratio $[D_{PMMA}/D_{LiF}]_{6MV}$ was calculated for the proposed phantom geometry in the calibration beam using a source model consisting of a (10×10 cm^2) parallel 6 MV x-ray photons by Sheikh-Bagheri and Rogers (41) for the specific linac model.

In low-energy BT sources, the ratio $[D_{PMMA}/D_{LiF}]_{^{125}I}$ can be estimated by the large cavity theory (LCT), in which the secondary electron ranges shorter than the cavity size in which the dose is calculated (42,43). Under the proposed conditions, the LiF (thickness 0.0254 cm) is approximately 10 times greater than the CSDA range of electrons in water ($R_{CSDA,35,5\ keV} \cong 2{,}5.10^{-3}$cm) for the maximum ^{125}I energy, which indicates the used LiF can be considered a large cavity.

According to LCT, and assuming there is charged-particle equilibrium (CPE) within the LiF at the proposed phantom, the ratio $[D_{PMMA}/D_{LiF}]_{^{125}I}$ can be approximated to the Eq. (4).

$$\frac{D_{PMMA}}{D_{LiF}} = (\bar{\mu}_{en}/\rho)_{LiF}^{PMMA}.\Psi_{LiF}^{PMMA} \tag{4}$$

where Ψ_{LiF}^{PMMA} is the energy-fluence ratio between PMMA and LiF, and $(\bar{\mu}_{en}/\rho)_{LiF}^{PMMA}$ is the ratio between $(\bar{\mu}_{en}/\rho)_{PMMA}$ and $(\bar{\mu}_{en}/\rho)_{LiF}$, that is, the PMMA to LiF ratio of the energy-fluence weighted average mass energy-absorption coefficients.

With this, we can rewrite the Eq. (5) as:

$$f^{rel} = \frac{f\left(^{125}I\right)}{f(6MV)} = \frac{\left[(\bar{\mu}_{en}/\rho)_{LiF}^{PMMA}.\Psi_{LiF}^{PMMA}\right]_{^{125}I}}{[D_{PMMA}/D_{LiF}]_{6MV}} \tag{5}$$

with factors MC-scored as described in Eqs. (6) and (7), respectively.

$$\Psi_{LiF}^{PMMA} = \frac{\int_{E_{min}}^{E_{max}} \Psi_{PMMA}(E)dE}{\int_{E_{min}}^{E_{max}} \Psi_{LiF}(E)dE} \tag{6}$$

where $\Psi_{PMMA}(E)$ and $\Psi_{LiF}(E)$ are the energy-fluence in PMMA and LiF, respectively, calculated by *F4 tally card throughout the energy range given by the minimum and maximum energy limits of the ^{125}I seed ($E_{min} = 1.0$ keV and $E_{max} = 35.492$ keV).

Following the same procedure, Eq. (7) was solved using tally *F4 associated with NIST coefficients (μ_{en}/ρ) (44) in the numerators and only *F4 in the denominators, as proposed by Giménez-Alventosa *et al.* (30) and references therein.

$$(\bar{\mu}_{en}/\rho)_{LiF}^{PMMA} = \frac{\frac{\int_{E_{min}}^{E_{max}} \Psi_{PMMA}(E).(\mu_{en}(E)/\rho)_{PMMA}dE}{\int_{E_{min}}^{E_{max}} \Psi_{PMMA}(E)dE}}{\frac{\int_{E_{min}}^{E_{max}} \Psi_{LiF}(E).(\mu_{en}(E)/\rho)_{LiF}dE}{\int_{E_{min}}^{E_{max}} \Psi_{LiF}(E)dE}} \tag{7}$$

Recent studies (7,9–13,45) 41 show that k^{rel} cannot be calculated directly by MC codes, as these calculations do not account for the signal formation process in the detector and the dependence of its efficiency on the linear energy transfer of the radiation, due to the solid-state nature of the LiF. Following the recommendation of the TG-43 (6), the k^{rel} value used is 0.931 $\pm$ 0.013, obtained from a global value for ^{125}I seeds by Rodrigues and Rogers (9).

Seeking a clearer understanding of the text, superscript indices will be used to designate the procedure adopted to

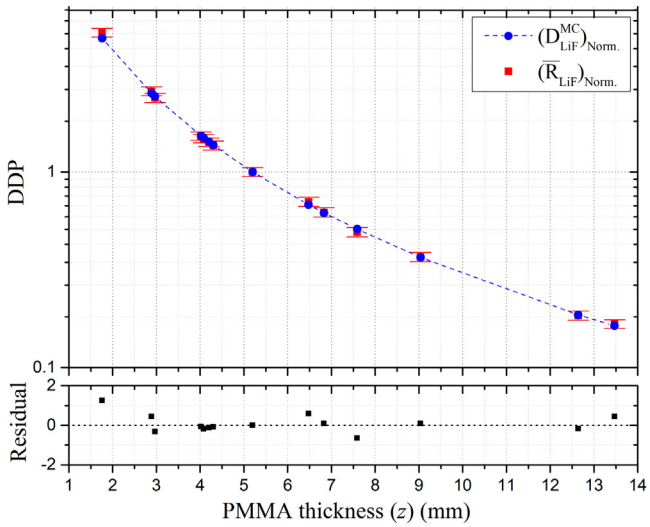

Fig. 2. Top - Relative Depth Dose Profile – DDP, using PMMA as the medium to perform the radiation transport: Simulated ($(D^{MC}_{LiF})_{Norm.}$- in blue) and experimental ($(\bar{R}_{LiF})_{Norm.}$- in red). Values are normalized to the thickness $z = 5.200 \pm 0.011$mm. Bottom – Residuals, taking simulated values as reference. (For interpretation of the references to color in this figure legend, the reader is referred to the Web version of this article.)

evaluate the dose: *conv* and *MC* to designate, respectively, the absorbed dose obtained from the conversion through cavity theory, and the absorbed dose calculated by MC simulation using *F8 tally card. In this way, D_{PMMA} of the Eq. (2) will be renamed to $D^{conv.}_{PMMA}$.

Data analysis

Comparisons of the experimental and calculation data were carried out through the residual graph. Such graphic allows the evaluation of the general behavior of the performed experiments and it is obtained according to Eq. (8) for Fig. 2.

$$residual_{(z)} = \frac{\left(\bar{R}_{LiF(z)}\right)_{Norm.} - \left(D^{MC}_{LiF(z)}\right)_{Norm.}}{\left(\sigma_{\bar{R}_{LiF(z)}}\right)_{Norm.}} \qquad (8)$$

where $(\bar{R}_{LiF(z)})_{Norm.}$ is the average of the normalized experimental values at each thickness z with its respective propagated uncertainty $(\sigma_{\bar{R}_{LiF(z)}})_{Norm.}$ and, $(D^{MC}_{LiF(z)})_{Norm.}$ is normalized calculated values by MC. In this way, the residuals are dimensionless.

Uncertainty budget

The estimated uncertainties associated with the experimental and calculated values are presented in Table 2, resulting in a maximum final total uncertainty of 5.68 %. The uncertainty of MC is the tally statistic for Type A and the seed geometry and energy spectrum for Type B, similar to Kennedy *et al.* (46) values.

Uncertainty values are reported using a coverage factor k = 1 (i.e., 1 σ). The type A uncertainty assigned to repetitive LiF measurements was estimated from the standard deviation of the mean value. TLD responses and uncertainties were measured for each one of the 14 PMMA thicknesses (z) evaluated in this work. Data were collected at an amount that suffice both the best estimate values, given by the average responses, and uncertainty estimates, given by the mean standard deviations.

Many parameters may contribute to the composition of the overall uncertainties involved in brachytherapy dosimetry measurements (47). A list of these data uncertainty players is presented in order to provide a general view of their contribution.

The uncertainty of the experimental measurements is the result of the combined effect of:

1- source strength: 4 batches of 10 sources each. No source was associated to a specific configuration parameter, such as PMMA thickness, LiF and LiF cavity holder positioning;
2- irradiation time uncertainty: irradiation time determined by setting a 1.5 mGy calculated air kerma value at 10 cm distance from the source, which corresponded to irradiation times ranging from 18h (new source) to 28h (at the end of source lifetime). Assembling and disassembling the irradiation setups took no longer than 30 seconds;
3- PMMA thickness: each slab was measured in different spots around its surface by at least 4 different experimenters. Their thicknesses were estimated by the mean values obtained from the results of set of 20 measurements on the average (14−28) performed for each thickness, which showed an overall 10.9 % (6.6%−13.0%) standard deviation. For the setup arrangements where more than one slab was used, uncertainty was estimated by the propagation of uncertainties of each slab assuming no correlation between them.
4- PMMA density: PMMA density was assumed according to the value provided by the manufacturer as 1.19 g/cm^3, as it was within the uncertainty of the measured experimental value. All PMMA used to build the phantoms were from a single manufacturer.
5- Phantom structures alignment: LiF holder cavity displacement from the central radial line in a parallel line to the PMMA spacer surface.
6- LiF holder oversize: the air gap between the LiF and the PMMA spacer lower surface.
7- Internal source displacement: the displacement of the source rod from the seed central axis. As the seed placed in the seed cavity lays horizontally on the PMMA, one might expect the downward dislocation of the Ag rod containing the ^{125}I radionuclides to the inner surface of the hollow encapsulation cylinder closest to the PMMA spacer.

Table 2
Analysis of the uncertainty associated. Random or statistical effects are described with Type A uncertainties and Type B uncertainties describe systematic effects.

Source of uncertainty	Dosimetric uncertainty (%)	
	Type A	Type B
Average of repetitive measurements	3.46[a]	
LiF dose calibration		3.82
Relative absorbed dose energy dependence, f^{rel}		1.68
Relative absorbed dose energy dependence, k^{rel}		1.40
Monte Carlo results	0.90	0.33
Quadratic sum	3.58	4.41
Combined total uncertainty ($k=1$)	5.68	

[a] for the maximum value found for the thickness of ($z=6.831 \pm 0.017$) mm.

8- LiF sensitivity: LiFs were selected prior to the beginning of the experiments to provide a better precision throughout the experiments. No individual LiF sensitivity determination was done neither an energy dependence response. LiFs were selected randomly among the disposed preselect group during irradiations either as reference background detectors or as irradiation dose monitors.
9- LiF reader efficiency: LiFs were read in a Harshaw 3500 TLD reader.

In order to perform a sensitivity analysis evaluating the effect of the geometry parameters (items 3−7 in the list above) on the experimental results, a series of simulations were carried out where the geometric differences on the ideal designed configuration were implemented one at a time. The chosen parameters are the ones associated solely to the phantom and source experimental configuration.

Results

Dose measurements

Figure 2 shows the experimental and simulated relative depth dose profiles (DDP) – respectively, $(\bar{R}_{LiF})_{Norm.}$ and $(D^{MC}_{LiF})_{Norm.}$ - as a function of the variation of PMMA thickness (z). Below these curves, the graph of residuals between them is presented (Eq. (8)), to assist in the analysis of the obtained results.

The experimental values, in red, corresponds to the average LiF response value obtained after a set of irradiations performed for each thickness. The uncertainties are given by the mean standard deviation. In general, to achieve similar uncertainties along all DDP range, a greater number of measurements were performed for the smallest thicknesses than have been for the thickest, as they are in a region closer to the seed and with a high dose gradient. For example, at thickness of $z=(1.763 \pm 0.016)$ mm the dose value corresponds to an average of 28 measurements, while at the largest thickness, $z=(13.470 \pm 0.025)$ mm, to an average of 10 measurements.

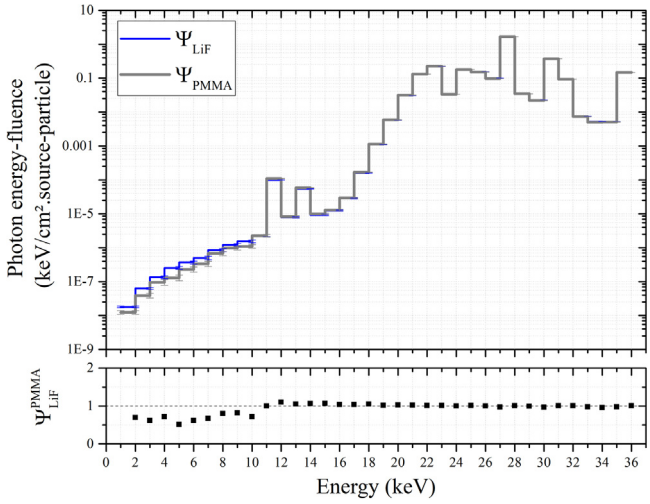

Fig. 3. Top: Calculated photon energy-fluence spectra in the detector cavity either filled with LiF (blue line) or filled with medium material, that is, PMMA (gray line), for an PMMA spacer thickness of $z=(5.200 \pm 0.011)$ mm; bottom: the corresponding energy-fluence ratio value Ψ^{PMMA}_{LiF}. (For interpretation of the references to color in this figure legend, the reader is referred to the Web version of this article.)

Relative absorbed-dose energy dependence f^{rel}

To support the assumption that the LiF is a large cavity when irradiated with ^{125}I seed, absorbed dose and collision kerma were estimated in the proposed phantom, using MCNP6.2 tallies *F8 and F6, respectively. The results present differences between tallies below 0.14 %, which are smaller than the tallied uncertainties (Type A), supporting the initial assumption.

$f(^{125}I)$ was estimated from the Ψ^{PMMA}_{LiF} and $(\bar{\mu}_{en}/\rho)^{PMMA}_{LiF}$ MC-scored quantities obtained according to Eqs. (6) and (7), respectively. The values of Ψ^{PMMA}_{LiF} were evaluated for each thickness (z) from the photon energy-fluence in the cavity (LiF or PMMA). Figure 3 shows the Ψ_{LiF} (blue color) and Ψ_{PMMA} (gray color) as a function of energy calculate for a $z=(5.200 \pm 0.011)$ mm PMMA thickness.

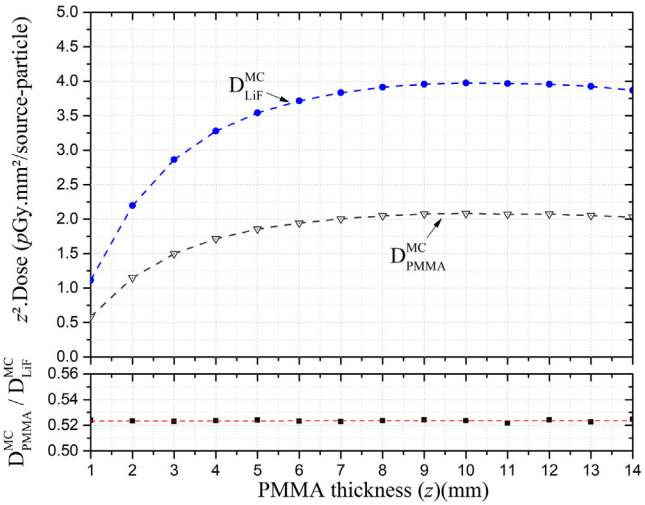

Fig. 4. Top: $D^{MC}_{LiF}(z)$ (blue dots) and $D^{MC}_{PMMA}(z)$(gray triangles) multiplied by square thickness value for different thicknesses (z) of PMMA; bottom: the corresponding calculated dose ratios, $D^{MC}_{PMMA}/D^{MC}_{LiF}$.

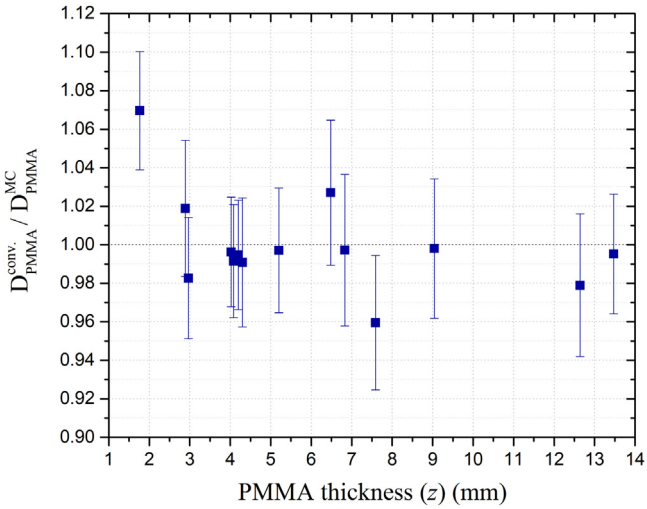

Fig. 5. Ratio between the converted and calculate absorbed dose to medium (PMMA).

LiF and PMMA calculated photon energy-fluence spectra overlap each other retrieving similar results, with differences within the statistical uncertainties, except for energies below 10 keV. The integral photon energy-fluence was calculated for both LiF and PMMA for all thickness. Performing these calculations for all the PMMA thicknesses used in the phantoms along this work leads to an average energy-fluence ratio value of $\Psi^{PMMA}_{LiF} = (1.0063 \pm 0.0010)$, with an uncertainty below 0.11 % obtained from the mean standard deviation.

The $(\bar{\mu}_{en}/\rho)^{PMMA}_{LiF}$ was evaluated, for each z, from the ratio of mass energy-absorption coefficients of PMMA and LiF, averaged over the local photon energy-fluence (Eq. (7)). The calculated values were constant for the different thicknesses (z) resulting in an average value of $(\bar{\mu}_{en}/\rho)^{PMMA}_{LiF} = (0.5201 \pm 0.0006)$.

To validate the obtained Ψ^{PMMA}_{LiF} and $(\bar{\mu}_{en}/\rho)^{PMMA}_{LiF}$ factors, D^{MC}_{LiF} and D^{MC}_{PMMA} were calculated for different PMMA thicknesses (z) from 1.0 mm to 14.0 mm range, in 1.0 mm increments. These estimates were multiplied by the square of the material thickness (z^2), so to have the square of distance geometric dependence factored out from the results, before been shown in Fig. 4. All dose values were estimated using tally *F8, retrieving estimates with Type A uncertainties below 0.2%.

In addition to dose profiles, Figure 4 shows the ratio $[D^{MC}_{PMMA}/D^{MC}_{LiF}]_{^{125}I}$, which exhibit a constant behavior as a function of thickness, consistent with the literature (42). This is due to the narrow range of the ^{125}I seed photon spectrum, with energies varying between 27.2 and 35.5 keV, thereby limiting the spectrum changes as a function of distance, especially, when compared to other low energy sources such as ^{103}Pd, which have a soft continuous spectrum and undergoes significant beam hardening as a function of distance (48).

The ratio $[D^{MC}_{PMMA}/D^{MC}_{LiF}]_{^{125}I}$ results in an average value of (0.5234 ± 0.0007), which corresponds to the product of $[(\bar{\mu}_{en}/\rho)^{PMMA}_{LiF}.\Psi^{PMMA}_{LiF}]_{^{125}I} = (0.5234 \pm 0.0008)$. The excellent agreement between these values shows the calculated $f(^{125}I)$ suitability, to convert the LiF experimental response into the PMMA dose estimate $\bar{R}_{LiF} \rightarrow D^{conv.}_{PMMA}$.

For high energy beam, the $f(6MV)$ parameter was estimated from the calculated dose ratio $[D^{MC}_{PMMA}/D^{MC}_{LiF}]_{6MV}$. It is observed that this factor does not change as a function of depth, in agreement with the literature (9,16). The value of f^{rel} obtained here is (0.475±0.008).

D^{conv}_{PMMA} versus D^{MC}_{PMMA}

The D^{conv}_{PMMA} values can be used to validate the D^{MC}_{PMMA} MC calculations, so that in ideal conversion should yield a ratio of $D^{conv}_{PMMA}/D^{MC}_{PMMA} = 1$. Figure 5 confirm this fact, where the ratios between $D^{conv}_{PMMA}(z)$ and $D^{MC}_{PMMA}(z)$ are shown, for all values of (z).

The uncertainties on the ratio values presented in Fig. 5 takes into account the propagation of all uncertainties associated with the LiF measurements and the MC uncertainties associated with both terms of the ratio.

Phantom sensitivity

Figure 6 shows the results of the sensitivity analysis where the results from the error implemented configuration are compared with the results driven from the ideal designed configuration, which were taken as the reference.

The studied sources of errors on planned LiF dose delivering were those associated to the source modelling and

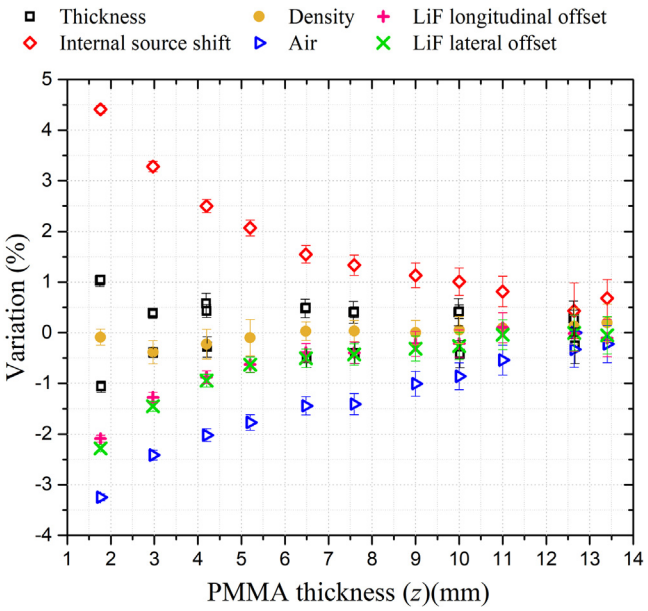

Fig. 6. Sensitivity analysis of phantom geometry parameters effect.

phantom construction and specification. Source modelling might be limited by an incorrect representation of the radiation source inside the seed. The downward displacement of the source inside the seed was evaluated as the seeds lay horizontally on the top slab of the phantom. Phantom construction might be subject to imperfections such as the misplacement of the LiF cavity holder out of the central position of the PMMA slab, leading to a misalignment between source and LiF, or even building an oversized cavity holder which might led to the formation of an air gap between the LiF and the spacer slab. Imprecisions on spacer slabs thicknesses and PMMA density are also a source of uncertainties. These errors were designated respectively as internal source shift; LiF (lateral and longitudinal) offset; air; thickness and density.

The air gap, LiF lateral and longitudinal offsets are associated to the displacement of the LiF from its planned position due to the misconstruction of the cavity holder, either by oversizing - leading to the presence of an air gap between the LiF and the variable thickness slabs - or by misplacing it on the slab surface - leading to LiF lateral and longitudinal offsets.

In this analysis, dose variations due to the thickness parameter (z) were compared to results driven for thicknesses increased (and decreased) by their respective mean standard deviation, that is, $z+s_z$ (and z-s_z). Their correspondent variations are depicted by black squares. LiF displacements were evaluated for an amplitude offset of 0.5 mm, longitudinally and laterally to the source. Variations for an air gap of 0.05 mm, corresponding to 20 % of the LiF thickness and variations due to a PMMA density decrement to 1.18 g/cm^3 (experimental value) were also evaluated.

Discussion

Phantom sensitivity analysis

A sensitivity analysis was performed in order to assess the designed phantom and identify the source of uncertainties and their influence on the performance of the entire experimental process. As expected, Figure 6 corroborates the largest sensitivity of the points associated to smallest thicknesses. This behavior was clear to all parameters except for the density change, which presented uncertainties as large as the calculated variations all along the thickness range.

The results may be gathered in 3 groups according to their behavior on the sensitivity analysis:

1- Positive sensitivity: parameters associated to changes which led to larger dose estimates than the reference configuration. These parameters are associated to the reduction of the reference source to detector distance such as observed for the internal displacement of the source rod inside the brachytherapy source, and the reduction of the assumed PMMA spacer thicknesses.
2- Negative sensitivity: parameters associated to changes, which led to smaller dose estimates than the reference configuration. These parameters are associated to the displacement of the LiF from its designed position: either by increasing the source to detector distance, such as the air gap parameter evaluation, or to dislocation of the LiF away from the source median central line, such as evaluated by the LiF offsets.
3- No apparent sensitivity: as the one represented by the density. This parameter might present a negative (positive) sensitivity for larger (smaller) densities, but showed no variations between the evaluated density values.

Data presented in Fig. 6 make it possible to evaluate/quantify the impact of possible errors in the experimental arrangement, in relation to the idealized experiment. In this sense, the estimated errors consist of limits associated with a specific irradiation configuration, while the experimental procedure were performed with different seeds and phantoms.

The individual errors are below the precision/reproducibility of the LiFs used, except for the errors of internal source shift and air, for smaller distances (z < 3 mm). However, these errors present opposite behaviors, which reduces their possible expressions. A specific study must be carried out to evaluate the downward displacement of the source inside the seed, which could justify the overresponse of the dose evaluated for the smallest distance, z = (1.763 ± 0.016) mm.

The phantom sensitivity analysis performed is a novelty in the way of evaluating the data obtained experimentally in relation to the other phantoms present in the literature.

It is worth noting that there are a variety of previous studies that present phantoms that seek to generate reference data for the TG-43 (6), from the experimental and/or calculated characterization of BT sources, with evaluations of the dose-rate constant, the anisotropy function, and the radial dose function in water or in water-like plastic (14,16,33,37,38,40). However, the proposal of this work differs from the others in methodological terms, introducing a novelty with a phantom that allows the generation of data for the TG-186.

The aim of this phantom was to develop a high-quality versatile design that is easily adapted to support different heterogeneous materials and experimental configurations. As it is formed by different sections (slabs), it is easily possible to adapt them to new compositions or measurements configurations.

Dose conversion analysis

The conversion of the experimental LiF response to the dose to medium is performed by the parameters f^{rel} and k_{bq}^{rel}. The $f(^{125}I)$ was obtained through Ψ_{LiF}^{PMMA} and $(\bar{\mu}_{en}/\rho)_{LiF}^{PMMA}$ MC-scored quantities. The Ψ_{LiF}^{PMMA} value (1.0063 ± 0.0011) was estimated from the average of the photon energy-fluence ratios in LiF and PMMA calculated for different thicknesses (z). This value can be approximated to unity, under all evaluated irradiation conditions, that is, $\Psi_{LiF}^{PMMA} \cong 1$ in all source-detector estimated distances, showing that the studied LiF hardly disturb the photon energy-fluence of the medium.

This approximation corroborates to the principle assumed by the LCT, so that, most studies (20,42,43) convert the dose from one medium to another using the ratio of mass energy-absorption coefficients only, $f(^{125}I) \approx (\bar{\mu}_{en}/\rho)_{LiF}^{PMMA}$, as done by Rodrigues and Rogers (9). On the other hand, Andreo (27,28) and Giménez-Alventosa *et al.* (30) report that the common assumption of considering approximately equal the energy-fluence in cavity and in medium is a poor approximation, especially for high Z tissues. Giménez-Alventosa *et al.* (30) present variations of 3.0 % for the tissue adipose/water ratio and 30.0 % for the bone/water ratio, using ^{125}I seed.

Keeping the recommendation in mind, we choose to keep the calculated Ψ_{LiF}^{PMMA} value in the $f(^{125}I)$, resulting in a more accurate conversion, in about 0.6 %, which turns to become more relevant for some phantom material compositions other than PMMA, as shall be addressed in a subsequent work. It is worth emphasizing, that the photon fluence spectra which were the weighting factors used in the evaluation of Ψ_{LiF}^{PMMA} are the same used to calculate $(\bar{\mu}_{en}/\rho)_{LiF}^{PMMA}$.

The $(\bar{\mu}_{en}/\rho)_{LiF}^{PMMA}$ MC-scored quantities were obtained from the photon energy-fluence weighted average and NIST $(\mu_{en}(E)/\rho)$ data, resulting in a constant value for all evaluated phantom spacer thicknesses. The relative uncertainty values vary within 0.02 % for the smallest thickness ($z = 1.763 \pm 0.016$ mm) to 0.11 % for the largest thickness ($z = 13.470 \pm 0.025$ mm). These uncertainties come from the MC-calculated photon spectra, see Fig. 3, since the uncertainties of the mass energy-absorption coefficients were disregarded.

In the analyses done in this work, we verified that $(\bar{\mu}_{en}/\rho)_{LiF}^{PMMA}$ does not vary with voxel size. However, as well as Ψ_{LiF}^{PMMA}, $(\bar{\mu}_{en}/\rho)_{LiF}^{PMMA}$ estimates are highly dependent on medium composition and density. Minimal changes on media specification, particularly composition, lead to great changes on the calculated results (21,49).

To verify the validity of the calculated $f(^{125}I)$, an approach, based on $[D_{PMMA}^{MC}/D_{LiF}^{MC}]_{^{125}I}$, was carried out. D_{PMMA}^{MC} and D_{LiF}^{MC} were tallied for many PMMA thicknesses and the correspondent ratios were calculated leading to the same value found for $f(^{125}I)$. It is worth mentioning the difference in the methodology used to calculate these values, the $[(\bar{\mu}_{en}/\rho)_{LiF}^{PMMA}.\Psi_{LiF}^{PMMA}]_{^{125}I}$ factors, were calculated from the photon fluence in the cavity, and $[D_{PMMA}^{MC}/D_{LiF}^{MC}]_{^{125}I}$ from the energy deposited in the cavity. The good agreement shows that the computed $f(^{125}I)$ is an accurate parameter for the conversion of the data obtained experimentally into absorbed dose to PMMA.

f^{rel} was calculated for the phantom, ^{125}I seed and LiF model used, resulting in a value of (0.475±0.008). Rodriguez and Rogers (9) show the importance of using f^{rel} values specific to the seed and LiF shape involved, getting values that may vary up to 8.6 % just by changing the LiF shape.

The LiF relative intrinsic energy dependence, k^{rel}, on the other hand cannot be obtained exclusively by simulation. According to TG-43 (6), it can only be determined experimentally if ones used MC to calculate f^{rel} and thereby extract k^{rel} from the measured value of S_D(absorbed dose calibration coefficient).

Nunn *et al.* (10) demonstrate that the measured relative LiF response as a function of photon energy differed by up to 13 % from MC calculations, at low photon energies from 12 keV to 145 keV. Moutsatsos *et al.* (16) uses k^{rel} value of 0.916, with 2.5 % uncertainty adapted from the work of Kennedy *et al.* (46), which is based on an unpublished result for ^{125}I seeds. More recently, Reed *et al.* (10) measured k^{rel} value of 0.870 with 1.4 % combined standard uncertainty ($k = 1$), for the radiation quality of ^{125}I relative to ^{60}Co, obtaining values lower than corresponding results of previous studies for comparable qualities, with justified differences due to the LiF handling (annealing and reading parameters).

We chose to use the value obtained by Rodriguez and Rogers (9), which presents a generalized value obtained from a rigorous literature review of experimental data for low-energy BT seeds, without considering differences in LiF handling protocols. However, TG-43 (6) suggests that the k^{rel} needs to be updated and to take into account the dependence on LiF shape and seed model, such as f^{rel}.

Based on the f^{rel} and k^{rel}, the D^{conv}_{PMMA} was obtained and compared with MC-calculated dose to PMMA (D^{MC}_{PMMA}), as shown in Fig. 5. It is observed that all points approach unity, within their respective uncertainties. It is worth mentioning the similarity between this figure and the residual graphs presented in the bottom part of Fig. 2. They both show the adherence of the experimental dose estimates to their calculated dose correspondents showing the accuracy and precision of the experimental dose estimates. However, the main point lies on the difference of their meaning: while Fig. 2 shows matching experimental results and calculated dose values in the LiF dosimeter - $(\overline{R}_{LiF})_{Norm.}$ and $(D^{MC}_{LiF})_{Norm.}$, respectively, Figure 5 shows matching converted experimental and calculated dose values for the material where the radiation transport is realized, that is, the PMMA – respectively.

The good behavior of the $D^{conv}_{PMMA}/D^{MC}_{PMMA}$ ratio, allows validating the values of absorbed doses to medium obtained from MC calculations. Overall, the accurate and laborious experimental procedure used in this work validated MC-calculations, given the excellent agreement of the experiment with the corresponding MC results. The $R_{LiF} \rightarrow D^{conv.}_{PMMA}$ conversion using cavity theory is one of the great interests of radiotherapy, since LiF are one of the most used dosimeters in clinical practice.

In this work the LiF response was converted into absorbed dose in a PMMA medium, however the proposed methodology can be easily extended to different media, such as materials equivalent to biological tissues, only by properly introducing the heterogeneity of the medium in the phantom and in its correspondent MC simulations. However, it is worth mentioning that such a conversion requires precise knowledge of the composition of the medium, in order to accurately estimate the $(\bar{\mu}_{en}/\rho)$factor. Uncertainty in the composition of the medium is directly extended to the uncertainties of $D^{conv.}_{medium}$.

Conclusions

Following the recommendations of the TG-186 regarding the need to design and implement relevant physical phantoms geometries with known materials to generate reference data, this work proposed the design and construction of a phantom for low-energy BT dose measurements. The proposed phantom is simple both in design as in its composition. Nonetheless, it may provide precise results at the expenses of a laborious experimental procedure, its easy setup reproducibility turned it possible to repeat the experimental arrangement and gather enough data to achieve the demanded precision in dose evaluations. Its cost effectiveness is also an important makeup parameter as it becomes feasible to carry on the experimental procedure with many phantoms simultaneously. Also, heterogeneous materials can be easily incorporated into the phantom, allowing dose measurements in such conditions.

The experimental measurements were exhaustive and required laborious and thorough work, but allowed final uncertainties of less than 5.68 %, which can be considered excellent for dosimetry with low-energy brachytherapy seed, especially due to the high dose gradient at short distances. The accuracy of this data made it possible to convert the responses into absorbed dose to PMMA and to validate the dose conversion factor methodology.

Converting the absorbed dose to LiF into dose to medium has been a matter of clinical interest since the advent of MBDCA, as it allows an indirect experimental validation of absorbed dose to medium. It is worth emphasizing that the dose conversion factor methodology uses parameters that can be included in any treatment planning system, in addition to be easily extended to other BT seeds, dosimeters and can be determined for different materials simply introducing different heterogenous materials into the phantom, which shall soon be presented in a following work.

Acknowledgments

PCGA acknowledges CNEN (Comissão Nacional de Energia Nuclear) for a research fellowship.

References

[1] Mckeever SWS. Thermoluminescence of Solids. Cabridge University Press, 2011. doi:10.1017/CBO9780511564994.

[2] Duragkar A, Muley A, Pawar NR, Chopra V, et al. Versatility of thermoluminescence materials and radiation dosimetry - a review. *Luminescence* 2019;34:656–665. doi:10.1002/bio.3644.

[3] Nath R, Anderson LL, Luxton G, Weaver KA, et al. Dosimetry of interstitial brachytherapy sources: recommendations of the AAPM Radiation Therapy Committee Task Group No. 43. *Med Phys* 1995;22:209–234. doi:10.1118/1.597458.

[4] Rivard MJ, Coursey BM, DeWerd LA, Hanson WF, et al. Update of AAPM Task Group No. 43 Report: A revised AAPM protocol for brachytherapy dose calculations. *Med Phys* 2004;31:633–674. doi:10.1118/1.1646040.

[5] Rivard MJ, Butler WM, DeWerd LA, Huq MS, et al. Supplement to the 2004 update of the AAPM Task Group No. 43 Report. *Med Phys* 2007;34:2187–2205. doi:10.1118/1.2736790.

[6] Rivard MJ, Ballester F, Butler WM, DeWerd LA, et al. Supplement 2 for the 2004 update of the AAPM Task Group No. 43 Report: joint recommendations by the AAPM and GEC-ESTRO. *Med Phys* 2017;44:297–338. doi:10.1002/mp.12430.

[7] Davis SD, Ross CK, Mobit PN, Van der Zwan L, et al. The response of lif thermoluminescence dosemeters to photon beams in the energy range from 30 kV x rays to ^{60}Co gamma rays. *Radiat Prot Dosimetry* 2003;106:33–43. doi:10.1093/oxfordjournals.rpd.a006332.

[8] Rogers DWO. General characteristics of radiation dosimeters and a terminology to describe them. Clinical dosimetry measurements in radiotherapy. Madison, WI: Medical Physics Publishing; 2009. p. 137–45.

[9] Rodriguez M, Rogers DWO. Effect of improved TLD dosimetry on the determination of dose rate constants for 125I and 103Pd brachytherapy seeds. *Med Phys* 2014;41:114301 15. doi:10.1118/1.4895003.

[10] Reed JL, Rasmussen BE, Davis SD, Micka JA, et al. Determination of the intrinsic energy dependence of LiF:Mg,Ti thermolumi-

nescent dosimeters for 125I and 103Pd brachytherapy source relative to 60Co. *Med Phys* 2014;41:122103. doi:10.1118/1.4901300.

[11] Nunn AA, Davis SD, Micka JA, DeWerd LA, et al. LiF:Mg,Ti TLD response as a function of photon energy for moderately filtered x-ray spectra in the range of 20-250 kVp relative to ^{60}Co. *Med Phys* 2008;35:1859–1869. doi:10.1118/1.2898137.

[12] Tedgren AC, Hedman A, Grindborg JE, Carlsson GA, et al. Response of LiF:Mg,Ti thermoluminescent dosimeters at photon energies relevant to the dosimetry of brachytherapy (<1 MeV). *Med Phys* 2011;38:5539–5550. doi:10.1118/1.3633892.

[13] Tedgren AC, Elia R, Hedtjarn H, Olsson S, Alm Carlsson G, et al. Determination of absorbed dose to water around a clinical HDR ^{192}Ir source using LiF:Mg,Ti TLDs demonstrates an LET dependence of detector response. *Med Phys* 2012;39:1133–1140. doi:10.1118/1.3675401.

[14] Perez-Calatayud J, Ballester F, Das RK, Dewerd LA, et al. Dose calculation for photon-emitting brachytherapy sources with average energy higher than 50 keV: report of the AAPM and ESTRO. *Med Phys* 2012;39:2904–2929. doi:10.1118/1.3703892.

[15] Gambarini G, Borroni M, Grisotto S, Maucione A, et al. Solid state TL detectors for in vivo dosimetry in brachytherapy. *Appl Radiat Isot* 2012;71:48–51. doi:10.1016/j.apradiso.2012.06.018.

[16] Moutsatsos A, Pantelis E, Papagiannis P, Baltas D. Experimental determination of the Task Group-43 dosimetric parameters of the new I25.S17 plus 125I brachytherapy source. *Brachytherapy* 2014;13:618–626. doi:10.1016/j.brachy.2014.07.001.

[17] Majdaeen M, Refahi S, Banaei A, Ghadimi M, et al. A comparison of skin dose estimation between thermoluminescent dosimeter and treatment planning system in prostatic cancer: a brachytherapy technique. *J Clin Transl Res* 2021;7:77–83. doi:10.18053/jctres.07.202101.006.

[18] Raffi JA, Davis SD, Hammer CG, Micka JA, et al. Determination of exit skin dose for 192Ir intracavitary accelerated partial breast irradiation with thermoluminescent dosimeters. *Med Phys* 2010;37:2693–2702. doi:10.1118/1.3429089.

[19] Adlienė D, Jakštas K, Urbonavičius BG. In vivo TLD dose measurements in catheter-based high-dose-rate brachytherapy. *Radiat Prot. Dosimetry* 2015;165:477–481. doi:10.1093/rpd/ncv054.

[20] Rivard MJ, Beaulieu L, Mourtada F. Enhancements to commissioning techniques and quality assurance of brachytherapy treatment planning systems that use model-based dose calculation algorithms. *Med Phys* 2010;37:2645–2658. doi:10.1118/1.3429131.

[21] Beaulieu L, Carlsson Tedgren A, Carrier JF, Davis SD, et al. Task Group 186 on model-based dose calculation methods in brachytherapy beyond the TG-43 formalism: current status and recommendations for clinical implementation. *Med Phys* 2012;39:6208–6236. doi:10.1118/1.4747264.

[22] Carlsson Tedgren A, Ahnesjö A. Optimization of the computational efficiency of a 3D, collapsed cone dose calculation algorithm for brachytherapy. *Med Phys* 2008;35:1611–1618. doi:10.1118/1.2889777.

[23] Van Veelen B, Ma Y, Beaulieu L. ACE advanced collapsed cone engine ELEKTA 2014. White paper available at Available at: www.elekta.com, Accessed June 29, 2022.

[24] Petrokokkinos L, Petrokokkinos L, Zourari K, Pantelis E, Moutsatsos A, et al. Dosimetric accuracy of a deterministic radiation transport based 192Ir brachytherapy treatment planning system. Part II: Monte Carlo and experimental verification of a multiple source dwell position plan employing a shielded applicator. *Med Phys* 2011;38:1981–1992. doi:10.1118/1.3567507.

[25] Lloyd SAM, Ansbacher W. Evaluation of an analytic linear Boltzmann transport equation solver for high-density inhomogeneities. *Med Phys* 2013;40:011707 -5. doi:10.1118/1.4769419.

[26] Branco ISL, Antunes PCG, Fonseca GP, Yoriyaz H. Monte Carlo studies on water and LiF cavity properties for dose-reporting quantities when using x-ray and brachytherapy sources. *Phys Med Biol* 2016;61:8890–8907. doi:10.1088/1361-6560/61/24/8890.

[27] Andreo P. Dose to 'water-like' media or dose to tissue in MV photons radiotherapy treatment planning: still a matter of debate. *Phys Med Biol* 2015;60:309–337. doi:10.1088/0031-9155/60/1/309.

[28] Andreo P. Dose to 'water-like' media or dose to tissue in MV photons radiotherapy treatment planning: still a matter of debate. *Phys Med Biol* 2015;60:2619 corrigendum.

[29] Ballester F, Carlsson Tedgren Å, Granero D, Haworth A, et al. A generic high-dose rate 192Ir brachytherapy source for evaluation of model-based dose calculations beyond the TG-43 formalism. *Med Phys* 2015;42:3048–3062. doi:10.1118/1.4921020.

[30] Giménez-Alventosa V, Antunes PC, Vijande J, Ballester F, et al. Collision-kerma conversion between dose-to-tissue and dose-to-water by photon energy-fluence corrections in low-energy brachytherapy. *Phys Med Biol* 2017;62:146–164. doi:10.1088/1361-6560/aa4f6a.

[31] Moura ES, Micka JA, Hammer CG, Culberson WS, et al. Development of a phantom to validate high-dose-rate brachytherapy treatment planning systems with heterogeneous algorithms. *Med Phys* 2015;42:1566–1574. doi:10.1118/1.4914390.

[32] Pappas EP, Zoros E, Moutsatsos A, Peppa V, et al. On the experimental validation of model-based dose calculation algorithms for ^{192}Ir HDR brachytherapy treatment planning. *Phys Med Biol* 2017;62:4160–4182. doi:10.1088/1361-6560/aa6a01.

[33] Taylor REP, Yegin G, Rogers DW O. Benchmarking BrachyDose: Voxel based EGSnrc Monte Carlo calculations of TG-43 dosimetry parameters. *Med Phys* 2017;34:445–457. doi:10.1118/1.2400843.

[34] Werner CJ, Bull JS, Solomon CJJ, Brown FB. et al. MCNP6.2 Release Notes, Los Alamos National Laboratory, report LA-UR-18-20808, 2018.

[35] Fonseca GP, Reniers B, Landry G, White S, et al. A medical image-based graphical platform - Features, applications and relevance for brachytherapy. *Brachytherapy* 2014;13:632–639. doi:10.1016/j.brachy.2014.07.004.

[36] Morato S, Juste B, Peris S, Miro R, et al. Brachytherapy organ dose estimation using Monte Carlo simulations of realistic patient models. *Annu Int Conf IEEE Eng Med Biol Soc* 2018;7:6149–6152. doi:10.1109/EMBC.2018.8513678.

[37] Dolan J, Li Z, Williamson JF. Monte Carlo and experimental dosimetry of an 125I brachytherapy seed. *Med Phys* 2006;33:4675–4684. doi:10.1118/1.2388158.

[38] Safigholi H, Chamberland MJP, Taylor REP, Allen CH, et al. Update of the CLRP TG-43 parameter database for low-energy brachytherapy sources. *Med Phys* 2020;47:4656–4669. doi:10.1002/mp.14249.

[39] Baglin CM. Nuclear data sheets for A = 192 Nucl. *Data Sheets* 2012;113:1871–2111.

[40] Taylor REP, Rogers DWO. An EGSnrc Monte Carlo-calculated database of TG-43 parameters. *Med Phys* 2008;35:4228–4241. doi:10.1118/1.2965360.

[41] Sheikh-Bagheri D, Rogers DWO. Monte Carlo calculation of nine megavoltage photon beam spectra using the BEAM code. *Med Phys* 2002;29:391–402. doi:10.1118/1.1445413.

[42] Landry G, Reniers B, Pignol JP, Beaulieu L, Verhaegen F, et al. The difference of scoring dose to water or tissues in Monte Carlo dose calculations for low energy brachytherapy photon sources. *Med Phys* 2011;38:1526–1533. doi:10.1118/1.3549760.

[43] Tedgren AC, Carlsson GA. Specification of absorbed dose to water using model-based dose calculation algorithms for treatment planning in brachytherapy. *Phys Med Biol* 2013;58:2561–2579. doi:10.1088/0031-9155/58/8/2561.

[44] Berger MJ 1994 ESTAR, PSTAR, ASTAR A PC packagea for calculating stopping powers and ranges of electrons, protons and helium ions Report IAEA-NDS-144

[45] Davis SD, Micka JA, DeWerd LA, Rasmussen B, et al. SU-GG-T-292: The response of LiF:Mg,Ti thermoluminescent dosimeters to low-energy photons. *Med Phys* 2008;35:2792. doi:10.1118/1.2962044.

[46] Kennedy RM, Davis SD, Micka JA, DeWerd LA, et al. Experimental and Monte Carlo determination of the TG-43 dosimetric parameters for the model 9011 THINSeedTM brachytherapy source. *Med Phys* 2010;37:1681–1688. doi:10.1118/1.3360899.

[47] DeWerd LA, Lbbott GS, Meigooni AS, Mitch MG, et al. A dosimetric uncertainty analysis for photon-emitting brachytherapy sources: report of AAPM task group No. 138 and GEC-ESTRO. *Med Phys* 2011;38:782–801. doi:10.1118/1.3533720.

[48] Liu D, Poon E, Bazalova M, Reniers B, et al. Spectroscopic characterization of a novel electronic brachytherapy system. *Phys Med Biol* 2008;53:61–75. doi:10.1088/0031-9155/53/1/004.

[49] Andreo P, Burns DT, Salvat F. On the uncertainties of photon mass energy-absorption coefficients and their ratios for radiation dosimetry. *Phys Med Biol* 2012;57:2117–2136. doi:10.1088/0031-9155/57/8/2117.